Journal of Materials Chemistry C

REVIEW

View Article Online
View Journal | View Issue

Cite this: J. Mater. Chem. C, 2019, 7, 12809

Emerging research directions for n-type conjugated polymers

Hanyu Jia[ab] and Ting Lei *[a]

Received 18th May 2019,
Accepted 1st July 2019

DOI: 10.1039/c9tc02632k

rsc.li/materials-c

In the past decade, π-conjugated polymers have been intensively studied in printed optoelectronic applications, such as organic field-effect transistors (OFETs) and organic photovoltaics (OPVs). After years of development, n-type conjugated polymers have exhibited comparable performance to that of their p-type counterparts in both OFETs and OPVs. Apart from OFET and OPV studies, several new research directions for n-type conjugated polymers recently appeared, including organic thermoelectrics, organic electrochemical transistors, organic spintronics, and organic energy storage systems. In these fields, n-type conjugated polymers are either less studied or their device performance lags far behind that of p-type ones. This review highlights the important role of n-type conjugated polymers in these emerging research directions and summarizes the recent progress in the development of n-type conjugated polymers in these new research fields. These fields require n-type conjugated polymers with new properties, such as better mixing with ionized dopants or good water permeability. Thus, new polymer design strategies and device engineering considerations are desired.

1. Introduction

Owing to their intrinsic advantages of light-weight, solution processability, and high mechanical flexibility, conjugated polymers have been developed for various optoelectronic applications, including organic field-effect transistors (OFETs) and organic photovoltaics (OPVs).[1–4] In OFETs, conjugated polymers are used as the channel materials for low-temperature processed thin-film transistors.[1,5–8] In OPVs, conjugated polymers have been used as either donor or acceptor materials.[3,9–11] In both fields, the development of p-type conjugated polymers is always faster and better than that of the corresponding n-type conjugated polymers. The first polymer FET[12] and the first bulk heterojunction OPV[13] were all reported using p-type conjugated polymers. This is mainly because most of the p-type conjugated polymer materials have suitable HOMO levels in the range of 4.9–6.0 eV, below the hole

[a] Key Laboratory of Polymer Chemistry and Physics of Ministry of Education, Department of Materials Science and Engineering, College of Engineering, Peking University, Beijing 100871, China. E-mail: tinglei@pku.edu.cn
[b] College of Chemistry and Molecular Engineering, Peking University, Beijing 100871, China

Hanyu Jia

Hanyu Jia obtained his BSc in chemistry from Zhengzhou University (China) in 2011. He received his PhD in polymer chemistry from Renmin University of China in 2018. He is currently a postdoctoral fellow at Peking University. His current research focuses on organic electrochemical transistors and their applications in flexible electronics and bioelectronics.

Ting Lei

Ting Lei is an assistant professor in the Department of Materials Science and Engineering at Peking University. He received his PhD from Peking University in 2013. After completing his postdoctoral training in Stanford, he joined Peking University in 2018. He has published more than 50 peer-reviewed papers on organic/polymer functional materials and optoelectronic devices. His current research focuses on organic/polymer functional materials, organic electronics, carbon-based electronics, and bioelectronics.

trapping energy level caused by oxygen and water redox reactions (−4.8 eV).[14,15] Thus, the hole transport is stable under ambient conditions. In addition, polymer building blocks with adequate HOMO levels are abundant, thus leading to the rapid development of p-type conjugated polymers. To date, p-type conjugated polymers have exhibited high charge carrier mobilities over 5 $cm^2 V^{-1} s^{-1}$, already surpassing the performance of the widely used TFT material, amorphous silicon (a-Si).[16–19] p-Type conjugated polymers are currently the dominant component in various types of OPVs, where dozens of p-type conjugated polymers have been developed, and some have exhibited high power conversion efficiency (PCE) over 16%.[20–22]

In OFETs, to enable a faster circuit speed, lower power consumption and more stable operation, an n-type polymer FET is necessary to construct CMOS-like circuits (Fig. 2a).[1,5,23] In OPVs, n-type conjugated polymers can be used as an acceptor to construct all-polymer solar cells that have better morphological stability, mechanical properties, and printing availability than OPVs containing small molecules (Fig. 2b).[10,24,25] To avoid O_2 and H_2O induced electron trapping and good charge injection from noble metals (*e.g.* Au) in OFETs and to match the electron-accepting ability in all-polymer OPVs, n-type conjugated polymers need to have low-lying lowest unoccupied molecular orbit (LUMO) levels, *e.g.* below −4.0 eV.[26–28] However, the development of n-type conjugated polymers is a tough journey because of the limited numbers of strong electron-deficient building blocks.

During the past few years, many efforts have been devoted to the design, synthesis, and device engineering of new n-type conjugated polymers. Several strong electron-deficient building blocks, including naphthalene diimide (NDI), benzothiadiazole (BT), diketopyrrolopyrrole (DPP), isoindigo (IID), benzobisthiadiazole (BBT), and benzodifurandione-based oligo(*p*-phenylene vinylene) (BDOPV), were developed with LUMO levels ranging from −3.4 eV to −4.2 eV (Fig. 1).[1,29] These building blocks can be further modified to achieve even lower LUMO levels, *e.g.* by introducing electron-withdrawing groups (*e.g.* F, Cl, *etc.*) on the polymer backbone.[30–33] Apart from structure engineering, device engineering strategies also significantly contributed to the performance enhancement of n-type OFETs.[34–36] To date, several n-type polymers have exhibited electron mobilities over 5 $cm^2 V^{-1} s^{-1}$ with good air-stability.[16,29,30,37–39] n-Type conjugated polymers are gradually replacing the fullerene-based acceptor as the novel non-fullerene acceptors in all-polymer OPVs; these all-polymer OPVs have exhibited PCE over 10%.[40] Therefore, in these fields, n-type conjugated polymers have exhibited comparable performance to that of their p-type counterparts. These achievements of n-type conjugated polymers in OFETs and OPVs have been very well summarized in several nice reviews.[10,41,42]

Apart from these traditional applications, some new research directions of conjugated polymers are attracting increasing attention, including organic thermoelectrics (OTEs), organic electrochemical transistors (OECTs), organic spintronics, and organic energy storage systems. In these new research fields, n-type conjugated polymers are either less studied or their device performance lags far behind that of their p-type counterparts. In this review, we will summarize recent developments of n-type conjugated polymers in these fast-developing or emerging directions, and discuss molecular design strategies and challenges in these research fields. We hope this review can provide basic concepts and molecular design strategies of n-type conjugated polymers, and push forward the study and development of n-type conjugated polymers in these new directions.

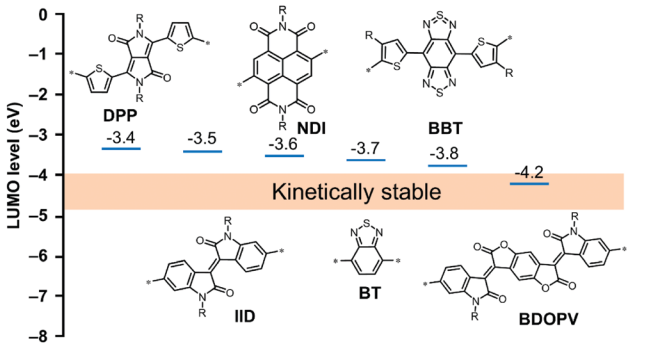

Fig. 1 Molecular structures and measured LUMO levels of several typical electron-deficient building blocks for n-type conjugated polymers. The kinetically stable range of the LUMO level is highlighted with an orange stripe.

2. n-Type conjugated polymer thermoelectrics

Thermoelectric (TE) materials can convert heat into electricity when they are placed with one end on the hot source and the other end on the cold source (Fig. 2c). Organic thermoelectric materials have attracted increasing interest due to their low thermal conductivity, low toxicity, light weight, high mechanical flexibility, and good solution processability compared to inorganic metallic alloys.[43] These intrinsic advantages render organic thermoelectrics the next-generation flexible and wearable energy harvesting and active cooling systems. The thermoelectric performance of thermoelectric materials is evaluated by a figure of merit, *ZT*. *ZT* is determined by Seebeck coefficient (S), electrical conductivity (σ), and thermal conductivity (κ) ($ZT = S^2\sigma T/\kappa$).[44] Considering the intrinsic low thermal conductivity of polymeric materials (0.3–1.0 W $m^{-1} K^{-1}$),[45] the power factor (PF = $S^2\sigma$) is frequently used to evaluate the thermoelectric performance of conjugated polymers.[46]

Like OFET and OPV fields, p-type thermoelectric polymers have been the most studied, including poly(3,4-ethylenedioxythiophene) (PEDOT), polythiophene derivatives (*e.g.* PBTTT), polyaniline (PANI), polypyrrole (PPy), polycarbazole, and poly(*p*-phenylene-vinylene) (PPV) derivatives.[47] Many p-type polymers have demonstrated high electrical conductivity over 100 S cm^{-1}. Among all the p-type polymers, PEDOT has shown the best thermoelectric performances with electrical conductivity over 1000 S cm^{-1} and power factor over 1000 μW $m^{-1} K^{-2}$.[48] Crispin *et al.* propose that the merging of the bipolaron network into the delocalized valence band contributes to the ultra-high

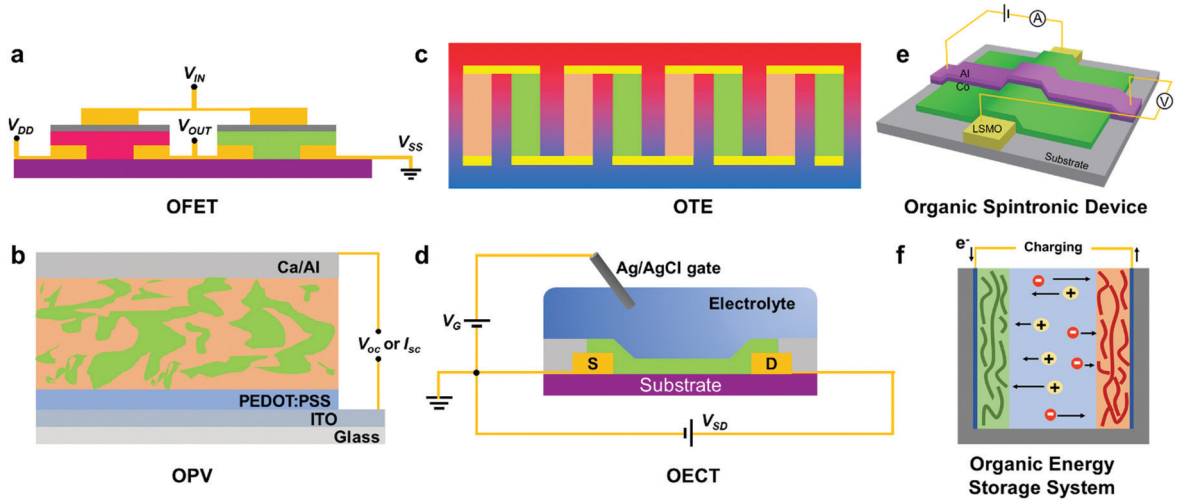

Fig. 2 Schematic illustration of various devices employing n-type conjugated polymers as one of their important components. (a) OFET, (b) OPV, and emerging new applications (c) OTE, (d) OECT, (e) organic spintronic, and (f) organic energy storage system. The p-type and n-type conjugated polymers in these applications are coloured red and green, respectively.

thermoelectric performance of the PEDOT:Tos system.[49] The *ZT* values of PEDOT were also reported in several papers, which are in the range of 0.2 to 0.4, comparable to that of the state-of-the-art inorganic materials at low temperature.[50,51]

To obtain a high thermoelectric conversion efficiency, both p- and n-type thermoelectric legs with comparable performance are needed.[52] Although the p-type thermoelectric materials have achieved high performance comparable to some of the inorganic materials, the development of n-type organic thermoelectric materials lag far behind that of the p-type ones. Among n-type polymer thermoelectric materials (Fig. 3a), powder-processed insoluble organometallic coordination polymers, poly(Ni 1,1,2,2-ethenetetrathiolate) derivatives, have exhibited good performances with electrical conductivity up to 40 S cm^{-1} and power factors up to 30 and 66 μW m^{-1} K^{-2}.[53] However, these materials are not readily solution-processed and lack the synthetic flexibility to further improve the polymer performance and processability, thus limiting their applications in large-area and low-cost thermoelectric devices.

The most used electron-deficient building block in solution-processable polymer thermoelectrics is NDI. Chabinyc *et al.* reported that mixing n-type polymer P(NDIOD-T2) (also named as N2200) with a dopant, namely (4-(1,3-dimethyl-2,3-dihydro-1*H*-benzoimidazol-2-yl)phenyl)dimethylamine (N-DMBI), leads to an electron conductivity of nearly 10^{-2} S cm^{-1} and power factors of up to 0.6 μW m^{-1} K^{-2} (Table 1).[54] Afterwards, Fabiano *et al.* used a "torsion-free" ladder-type NDI derivative, BBL, for n-type thermoelectrics (Fig. 3b).[55] BBL showed a much-improved electrical conductivity of up to 0.42 S cm^{-1} after exposing in the atmosphere of an n-type dopant, tetrakis(dimethylamino)ethylene (TDAE). Their theoretical calculation suggested that BBL showed a longer polaron delocalization length on the polymer backbone than N2200, leading to higher electrical conductivity and TE performance.

Pei *et al.* reported a series of BDPPV-based n-type conjugated polymers, exhibiting a high conductivity of up to 14 S cm^{-1} and

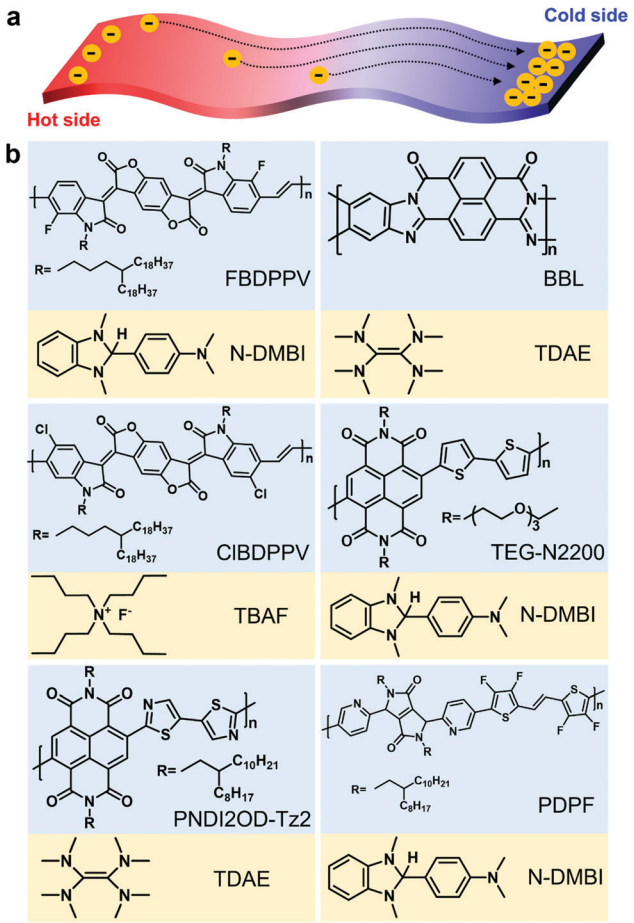

Fig. 3 (a) Schematic illustration of electron carrier directional diffusion of an n-type conjugated polymer placed upon the established thermal gradient. (b) Chemical structures of several typical n-type conjugated polymers and the corresponding dopants for high-performance n-type thermoelectrics.

Table 1 Summarized thermoelectric properties of n-type conjugated polymer based thermoelectrics

Polymer	Dopant	σ (S cm^{-1})	S (μV K^{-1})	PF (μW m^{-1} K^{-2})	Ref.
PNDI2OD-T2	N-DMBI	0.008	−850	0.6	54
BBL	TDAE	0.42	−101	0.43	55
FBDPPV	N-DMBI	14	−141	28	56
ClBDPPV	TBAF	0.62	−99.2	0.63	57
PNDI2OD-Tz2	TDAE	0.1	−447	1.5	59
TEG-N2200	N-DMBI	0.17	−160	0.4	58
PDPF	N-DMBI	1.3	−235	4.65	46

a power factor of 28 μW m^{-1} K^{-2} after doping with a certain amount of n-type dopant N-DMBI. Notably, fluorination of the BDPPV acceptor exhibited the best performance because it has a low LUMO level down to −4.17 eV, and thus can be more readily doped, leading to improved doping efficiency and higher charge carrier concentration than non-fluorinated BDPPV and chlorinated BDPPV polymers.[56] Based on chlorinated BDPPV, Katz *et al.* used TBAF as an air-stable, solution-processable n-type dopant to dope the chlorinated BDPPV, and obtained an electron conductivity of 0.62 S cm^{-1} and a power factor of 0.63 μW m^{-1} K^{-2}.[57] The doping mechanism is F^- anion addition, followed by an electron transfer process between F^- anion and ClBDPPV polymer. Interestingly, they found that TBAF doped ClBDPPV polymer thick films exhibited good air-stability, but the film electrical conductivity still decreased by 50% within 24 hours. Many studies have suggested that the low conductivity of the n-type conjugated polymer after doping is largely due to the poor miscibility between the polymer and the ionized dopant. To solve this issue, Koster *et al.* modified the NDI-based polymer N2200 with polar glycol side chains to replace the commonly used alkyl side chains (Fig. 3b). This strategy largely enhanced the dispersity of the n-type dopant in the polymer matrix, which was supported by molecular dynamics simulations (Fig. 4a and b). The highly dispersed n-type dopant can realize close contact with the polymer chain, thereby improving the doping efficiency. This strategy leads to a 200-fold enhancement in the conductivity of TEG-modified TEG-N2200 compared with the unmodified N2200 with alkyl side chains, implying an alternative route to enhance the thermoelectric performance of n-type conjugated polymers.[58]

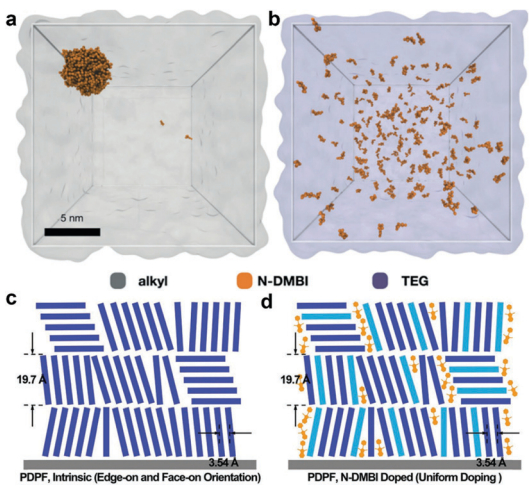

Fig. 4 Simulated dopant N-DMBI distribution in two n-type conjugated polymer phases with different side-chains: (a) the alkyl side-chain and (b) the glycol side-chain.[58] Schematic illustration of molecular packing modes of (c) pure PDPF and (d) N-DMBI doped PDPF.[46] Reprinted with permission from ref. 46 and 58, copyright 2018 Wiley-VCH.

Very recently, Pei *et al.* reported a donor engineering strategy to enhance the thermoelectric performance of DPP-based polymers.[46] Fluorine atoms were introduced into the donor moieties of a DPP polymer, which further decreased the polymer's HOMO and LUMO level. When doped with N-DMBI, fluorinated polymer PDPF (Fig. 3b) exhibited a significantly enhanced dopant miscibility than non-fluorinated polymer PDPH (Fig. 4c and d). The improved charge carrier concentration brought by higher doping efficiency led to a high conductivity of up to 1.3 S cm^{-1} and a power factor of 4.65 μW m^{-1} K^{-2}. These values are 1000 times higher than that of unmodified polymer PDPH. A similar strategy was also reported by Facchetti *et al.* They used an electron-deficient bithiazole donor unit to replace the bithiophene unit in polymer N2200 to enhance the doping efficiency (Fig. 3b, PNDI2OD-Tz2). The introduction of the electron-deficient bithiazole moiety enhanced the planarity of the polymer backbone, lowered the polymer's LUMO level, and led to a higher conductivity of 0.1 S cm^{-1} and a higher power factor of 1.5 μW m^{-1} K^{-2} compared to that of N2200.[59]

Based on the above examples, we can conclude that the thermoelectric performances of n-type conjugated polymers are still low, with the power factors of n-type conjugated polymers being at least one order of magnitude lower than that of p-type polymers. Since the Seebeck coefficients of p-type and n-type polymers are close, the major issue for n-type conjugated polymers is their low electrical conductivity. To enhance the conductivity, several strategies have been employed, including using electron-deficient building blocks and electron-withdrawing functional groups, introducing rigid "ladder-type" backbones, and replacing alkyl side chains with polar glycol side chains. However, the conductivity is still two orders of magnitude lower than that of the current state-of-the-art p-type polymers. In addition, we should note that few articles focused on the air stability of n-type polymer materials, which is critical for their practical applications.[57,60] Therefore, more endeavour is needed to further enhance the thermoelectric performances of n-type conjugated polymers.

3. n-Type organic electrochemical transistors

The organic electrochemical transistor (OECT) is a type of three-terminal transistor, which exploits the simultaneous ionic and electronic transport in organic semiconductors to realize remarkable current modulation (Fig. 2d). Since the channel material in OECTs directly contacts an aqueous environment and has good ion permeability and high transconductance, OECTs have been

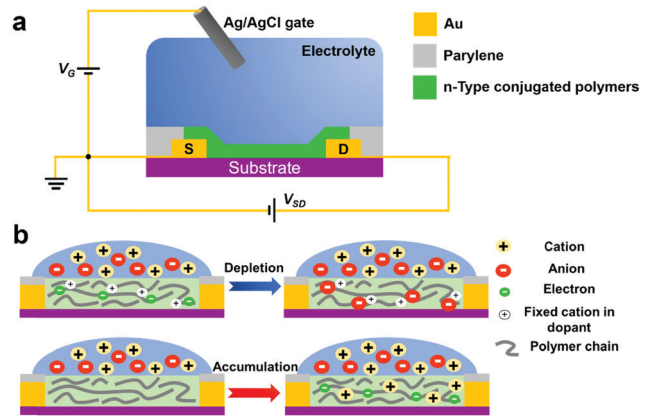

Fig. 5 (a) Schematic illustration of a typical device architecture of an OECT. (b) Electrochemical doping mechanism of a depletion-mode and an accumulation-mode OECT (using an n-type polymer as an example).

used in bioelectronics, neuromorphic computing, artificial synapses, and logic circuits.[61–66] As shown in Fig. 5a, a typical OECT consists of two metallic electrodes serving as the source and drain respectively, a parylene layer protecting electrodes from the electrolyte to avoid unfavoured electrochemical reactions, a semiconducting polymer layer as the channel material that directly contacts an electrolyte, and an Ag/AgCl reference electrode functioning as the gate. Different from the conventional electrolyte-gated OFETs (EGOFETs) that only induce interfacial charge carriers at the electrolyte–channel interface, in OECTs, the applied voltage bias on the Ag/AgCl gate can effectively drive cations or anions penetrating into the bulk of the polymer matrix in the channel.[64,67–69] This process results in electrochemical doping or dedoping of the bulk polymer channel, leading to remarkable current modulation of the polymer channel (Fig. 5b). Therefore, although EGOFETs have exhibited much higher capacitances (1–10 μF cm^{-2}) compared with traditional OFETs (10–100 nF cm^{-2}) due to accumulated ions at the electrolyte–semiconducting layer interface, their capacitances are still lower than that of the OECTs having effective bulk gating (up to 500 μF cm^{-2}).[64] When the conjugated polymer in the channel is intrinsically doped by small molecules, polyelectrolytes, or themselves, the OECT works in depletion mode,[70] whereas the OECT employing an undoped conjugated polymer as the channel works in accumulation mode.

To facilely judge and compare the performance of OECTs based on various conjugated polymers, transconductance g_m was proposed to evaluate the drain current modulation degree of the gate voltage and calculated as the first derivation of the transfer curve, namely,

$$g_m = \frac{\partial I_d}{\partial V_g}$$

Based on Bernard's model,[71] the transconductance g_m of an OECT in the saturation regime is determined by several parameters, including three channel dimensions of length L, width W, and film thickness d, charge carrier mobility μ, volumetric capacitance C^*, and threshold voltage V_{Th}. The relationship among these parameters is as follows:

$$g_m = \frac{W}{L} \cdot d \cdot \mu \cdot C^* \cdot (V_{Th} - V_g)$$

Obviously, the electrochemical doping throughout the channel remarkably improves the specific capacitance of the conjugated polymer in the channel, namely the product of thickness and volumetric capacitance ($d \cdot C^*$), leading to an extremely high transconductance of millisiemens, over 10^3-fold higher than that of EGOFETs.[64]

Until now, the most widely used channel material for OECTs is poly(3,4-ethylenedioxythiophene):poly(styrene sulfonate) (PEDOT:PSS). Its high transconductance and good ambient stability render PEDOT:PSS the optimal candidate in various OECT-based applications. Notably, in 2018, Yoon *et al.* reported that a concentrated H_2SO_4 treated PEDOT:PSS channel material exhibited an ultrahigh transconductance of 20 mS with channel dimensions of W/L = 80 μm/20 μm and d = 200 nm. The authors proposed that the high transconductance is benefited from the facile ion permeability through the highly ordered PEDOT:PSS crystalline region and nanopores led by the acid treatment.[72] PEDOT:PSS is intrinsically doped and operates in depletion mode, which is undesirable for applications requiring high current on/off ratios. Recently, the development of new p-type OECT materials working in the accumulation mode has attracted increasing interest. After introducing glycol side chains to enhance the ion penetration, several thiophene-based semiconducting polymers were successfully demonstrated with high transconductance in accumulation mode.[73–77] For example, p(g2T-TT), a polymer based on the PBTTT backbone with grafted glycol side chains, exhibited an even higher OECT transconductance than PEDOT:PSS.[74]

n-Type OECTs are a necessary component to construct complementary logic circuits (paired with p-type ones), which allow more complex bioelectronics with significantly reduced static power consumption.[78] However, n-type OECTs are still at their infant stage because n-type conjugated polymers are sensitive to O_2 and H_2O in an ambient environment, and they usually have limited hydrophilicity in that ions can hardly transport into the bulk channel.[64,78] To overcome these bottlenecks, a deep LUMO level (lower than −4.0 eV) and high hydrophilicity of n-type conjugated polymers are desired to construct high-performance n-type OECTs. In particular, when operating in aqueous solution, the applied gate and drain voltages of OECTs should be restricted to a small range to prevent water electro-oxidation and electro-reduction. Concretely, the upper and lower limit of the voltage applied between the gate and drain cannot exceed 0.89 V or be below −1.23 V (Fig. 6b).[78,79]

Compared with conventional n-type conjugated polymers that can only be used in "dry state", OECT polymers need to contact an aqueous electrolyte, and thus are required to have good hydrophilicity. Giovannitti *et al.* found after replacing the alkyl side chains with glycol chains and introducing glycol side chains on the thiophene units of the N2200 polymer (Fig. 6a),

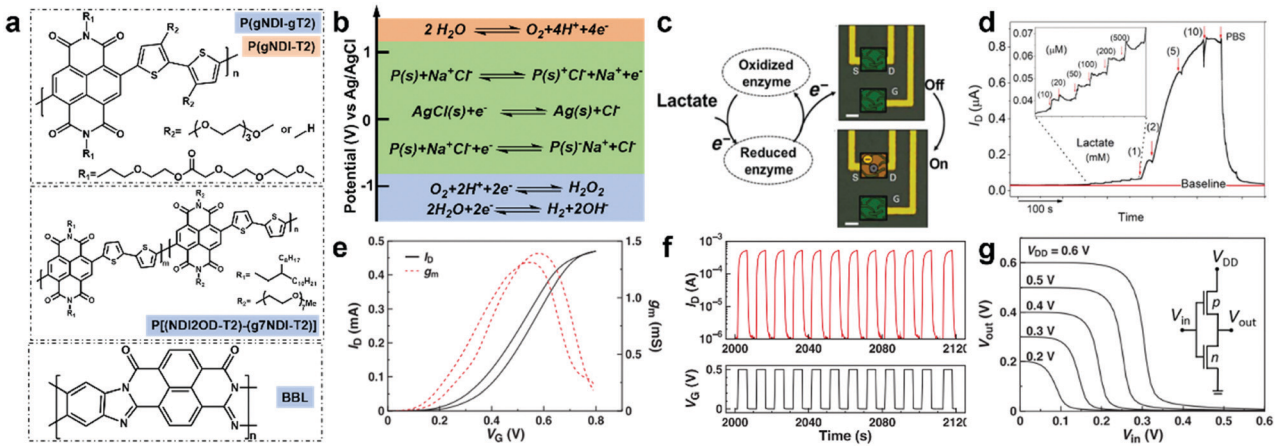

Fig. 6 (a) Chemical structures of several typical n-type conjugated polymers employed in organic electrochemical transistors. (b) Dominant electrochemical redox process upon different gate voltage range *versus* Ag/AgCl reference. (c) Mechanism of lactate sensing based on n-type OECTs. (d) Temporal drain current variation of the OECT sensor upon continuous addition of lactate with different concentrations.[81] Reprinted with permission from ref. 81, copyright 2018 AAAS. (e) Typical n-type transfer and transconductance curves of the BBL-based OECT. (f) Long-term operation stability of BBL upon the square-wave pulse of V_G. (g) Input–output characteristics of a complementary-type inverter based on the combination of p-type and n-type OECTs.[62] Reprinted with permission from ref. 62, copyright 2018 Wiley-VCH.

ion transport in the polymer can be significantly improved, though the polymer exhibited ambipolar charge transport in 0.1 M NaCl solution.[79] Compared with the polymer of P(gNDI-T2) with an unmodified bithiophene unit, more glycol side-chain density on P(gNDI-gT2) remarkably facilitates the ion migration process throughout the polymer channel, gaining a maximum transconductance of 21.7 μS with channel length L = 10 μm, width W = 100 μm, and film thickness d = 200 nm. Moreover, P(gNDI-gT2) exhibited stable in-water electrochemical operation for more than 2 hours, suggesting its potential application in the long-term recording of biological signals.

Subsequently, Giovannitti *et al.* systematically investigated the influence of the glycol grafting degree of the NDI-based polymer on the working regime in aqueous solution. In Fig. 6a, the n-type polymer P((NDI2OD-T2)-(g7NDI-T2)) consists of a hydrophobic, alkyl side-chain grafted NDI acceptor unit and a hydrophilic, polar glycol side-chain grafted NDI acceptor unit, connected with bithiophene as the donor unit. The ratio between glycol-NDI and alkyl-NDI determines the working mode of this n-type conjugated polymer since the glycol side-chain facilitates ion permeation into the polymer matrix and directly influences the OECT performance. The polymer with 0% glycol side chains (or 100% alkyl side chains) was named as P0, and the polymer with 100% glycol side chain was named as P100. They found that polymer P50 with 50% glycol side chains starts to exhibit the OECT property and P90 reaches the optimal performance based on the transconductance value. However, it is noteworthy that the gradually increasing ratio of the glycol side-chain remarkably impairs the electron mobility of the conjugated polymer, although gaining a higher capacitance. A delicate balance of electron mobility and capacitance should be made to obtain the highest transconductance, which leads to the highest transconductance in P90.[80]

Since P90 showed the optimal OECT performance, Owens and Inal *et al.* employed this polymer as the active material of OECTs for the specific and accurate metabolite sensing application. Concretely, P90 was spin-coated on the gate and the channel of an OECT, and further modified by the enzyme lactate oxidase (LOx) without employing any mediators and reference electrodes. This enzyme-based n-type OECT works in accumulation mode, guiding the electron generated by enzyme catalysis of lactate to the polymer channel and leading to a drain current response of the P90-based OECT (Fig. 6c). The introduction of LOx bestows the n-type OECT with high specific sensitivity to lactate. A rational setup of the gate and drain voltages of P90-based OECTs could detect a wide concentration range of lactate (10^{-5}–10^{-2} M), and the detection limit could reach as low as 10 μM (Fig. 6d). The application of n-type OECTs for metabolite sensing is likely to open up a novel platform for biomedical diagnosis with integrated microfluidic technology and wearable electronics.[81]

Recently, Fabiano *et al.* used the ladder-type conjugated polymer BBL for n-type OECTs. Taking advantage of the intrinsically high electron affinity, BBL-based OECTs exhibited excellent operation stability and electrochemical reversibility in aqueous solution (Fig. 6e–g). Notably, the BBL-based OECT possesses a high transconductance up to 9.7 mS with very large channel dimensions of W/L = 39 000 μm/20 μm and a film thickness of d = 180 nm. Combining with a typical p-type OECT polymer, namely poly(3-carboxy-pentyl-thiophene) (P3CPT), the authors demonstrated the first complementary-type inverter based on p- and n-type OECTs, and the inverter showed high gains under electrochemical operation.[62]

Clearly, n-type conjugated polymers applied in OECTs require good hydrophilicity to facilitate ion penetration into the bulk polymer channel upon applying a gate voltage. Side-chain engineering seems to be a very good approach to gain enough water and ion permeation. However, the introduction of hydrophilic glycol side-chains on polymers is not beneficial for gaining high electron mobility in aqueous solution.

The trade-off between electron mobility and ion penetration in n-type conjugated polymers should be considered to achieve optimal OECT performance. Notably, device engineering also strongly influences the device performance of OECTs. For example, the vertical OECT has greatly pushed the transconductance of the PEDOT:PSS-based p-type OECT to 57 mS, which may also be applicable to n-type OECTs.[82] Additionally, almost all n-type conjugated polymers employed in OECTs are undoped, and these n-type OECTs work in accumulation mode. Therefore, exploring intrinsically n-doped polymers is another interesting topic.

4. n-Type conjugated polymers for spintronics

Organic materials only contain light atoms that have weak spin–orbital interactions, and thus they are expected to have long spin lifetimes. To date, organic spintronic devices such as spin-valves, spin-OLEDs, and spin photovoltaics have been explored.[83–85] Spintronic devices adopt either the lateral structure[86] or the vertically sandwiched structure,[87] as shown in Fig. 7a and b. These structures are composed of two ferromagnetic (FM) electrodes separated by a layer of organic semiconductor spacer. Among various ferromagnetic electrode materials, LSMO ($La_{2/3}Sr_{1/3}MnO_3$) and Co are often employed either due to their high spin-polarization at their Fermi level or due to good processability.[87] These ferromagnetic electrode materials usually have relatively low work functions, ranging from 4.5 to 4.9 eV. Concretely, spins are injected from one FM electrode polarized by a magnetic field; the spins travel through the organic spacer *via* the thermal/field assisted tunnelling/hopping process under a given bias, and are finally detected by the other FM electrode. The parallel or opposite polarization on the two FM electrodes can be achieved by applying magnetic fields with different directions and strengths, leading to a huge resistance change measured on the two FM electrodes. This resistance change is named as the magnetoresistance (MR) effect. The MR can thus be calculated using the formula given below:[88,89]

$$\mathrm{MR} = \frac{2P_1P_2e^{-(d-d_0)/\lambda_s}}{1-P_1P_2e^{-(d-d_0)/\lambda_s}}$$

where P_1 and P_2 represent the generated and detected spin polarization on the two FM electrodes, respectively, d is the spacer width in the lateral configuration or thickness in the vertical configuration, d_0 is the FM metal diffusion depth in the spacer, also called the ill-defined layer, and λ_s is the spin diffusion length in the spacer. Obviously, high MR response can be obtained through the higher spin diffusion length (λ_s) and the smaller thickness (d) of the organic spacer. Furthermore, the spin diffusion length (λ_s) in the organic spacer is determined by carrier mobility (μ), spin relaxation time (τ), and operation temperature (T) and follows the equation given below:

$$\lambda_s = \sqrt{\mu k_B T \tau / e}$$

where k_B and e are the Boltzmann constant and carrier charge, respectively. Therefore, conjugated polymers are emerging as a novel type of spacer materials owing to their long spin relaxation time, profited from their weak spin–orbit coupling[90] and hyperfine interaction.[91] However, the conjugated polymer-based spacer in spin-valve devices still suffers from low spin diffusion length, caused by low carrier mobility and mismatched energy level with the Fermi level of contacted ferromagnetic electrodes, limiting their further application and performance enhancement in spintronics.

n-Type conjugated polymers possess a tunable LUMO level through electron-withdrawing group modification and side-chain engineering, which makes them easier to match the Fermi level of FM electrodes and further improve the injection efficiency of the spin-polarized electron from the FM electrode to the organic spacer.[89,92] Tunable molecular packing mode also improves the bulk carrier mobility in n-type conjugated polymers, contributing to gaining a longer spin diffusion length and then a higher MR response even at room temperature.[93,94] Moreover, n-type conjugated polymers could not only be employed in spin-valves as the spacer material but also potentially be adopted in spin photovoltaics to convert light irradiation into output current on applying a voltage and magnetic field with a specific orientation.

Recently, Zhang *et al.* developed a spin-valve device with a vertical configuration based on the n-type conjugated polymer P(NDI2OD-T2) (Fig. 8a). The polymer showed an extremely high MR response even at room temperature through the optimized interface structure of a spin-valve device. The LUMO level of P(NDI2OD-T2) is −4.0 eV, which is quite close to the Fermi level of LSMO and Co (Fig. 8b). The matched energy level between the two FM electrodes and the n-type conjugated polymer spacer largely impairs the interfacial barrier and facilitates spin-polarized electron injection. Moreover, the excellent air-stability of P(NDI2OD-T2) renders it a suitable polymeric spacer

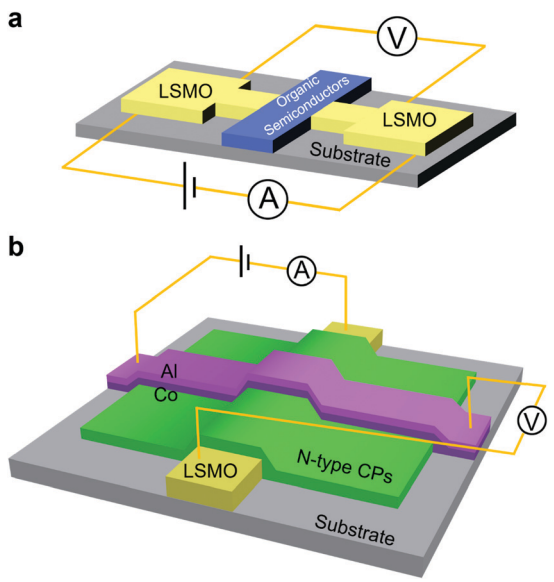

Fig. 7 Two typical device configurations adopted in spintronic devices, including (a) laterally sandwiched structure and (b) vertically sandwiched structure.

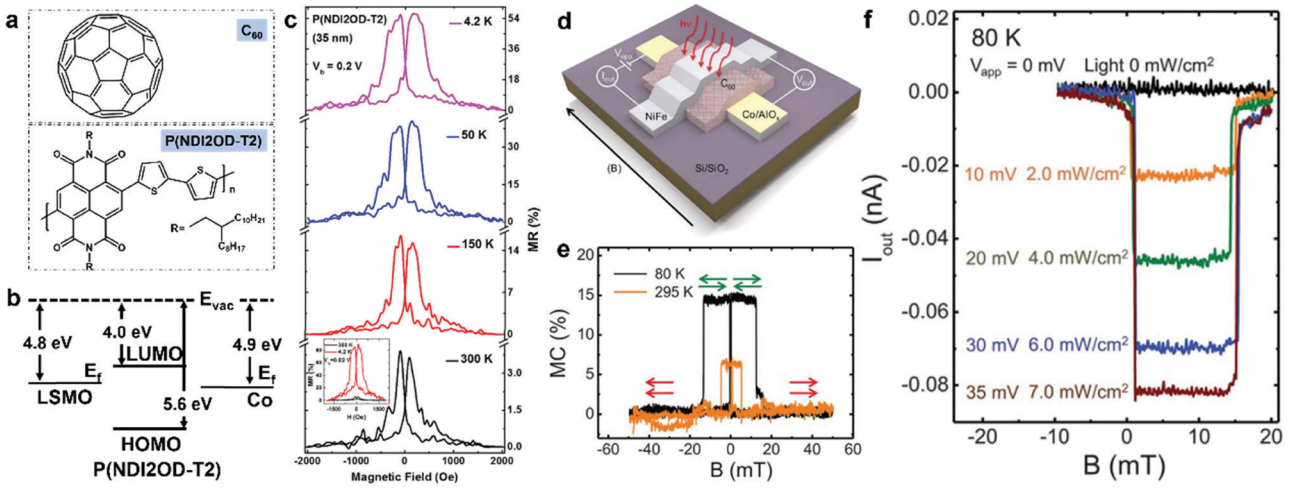

Fig. 8 (a) Chemical structures of n-type conjugated polymer P(NDI2OD-T2) and fullerene used in spintronic devices. (b) Fermi levels of ferromagnetic electrodes LSMO and Co, and the LUMO–HOMO levels of P(NDI2OD-T2). (c) The temperature dependent MR curve of the spin-valve with P(NDI2OD-T2) spacer upon different operation temperatures, including 4.2 K, 50 K, 150 K and 300 K (R.T.). The applied voltage bias is 0.2 V. The inset shows the MR curve of the same device operated with a voltage bias of 0.02 V.[89] Reprinted with permission from ref. 89, copyright 2018 Springer. (d) Schematic illustration of a C_{60}-based spin-photovoltaic device. (e) Magnetocurrent of the spin-photovoltaic device as a function of the magnetic field upon different operation temperatures of 80 K and 295 K. The applied voltage bias was 0.01 V and the device was measured without light irradiation. (f) The spin-polarized photogenerated current of the spin-photovoltaic device at 80 K with different applied voltages and light irradiation conditions.[85] Reprinted with permission from ref. 85, copyright 2018 AAAS.

in the organic spin-valve. Although the MR ratio of the P(NDI2OD-T2)-based spin-valve shows a strong temperature dependence (Fig. 8c), the MR signal of the spin-valve with an inserted AlO_x layer at the polymer–Co interface still can reach as high as 90% at 4.2 K and 6.8% at 300 K. Moreover, long spin relaxation length with a weak temperature dependence was also found to exist in P(NDI2OD-T2), making it possible to possess a highly efficient spin transport when employed as a spintronic material.[89]

Heuso *et al.* developed a C_{60} fullerene-based spin photovoltaic device with a similar structural configuration of a vertical-type spin-valve, as shown in Fig. 8d.[85] In principle, the C_{60} layer preserves the injected spin-polarized electrons from the Co electrode and transports these carriers to another FM electrode ($Ni_{80}Fe_{20}$) for spin detection. The process discussed above results in a remarkable current change, also called magnetocurrent (MC), on the $Ni_{80}Fe_{20}$ electrode on applying a magnetic field with a specific orientation. The optimized MC value of the spin photovoltaic device could reach ~15% at 80 K and 6.5% at 295 K when the two FM electrodes were anti-parallel polarized. Considering the intrinsically light-induced charge separation of the C_{60} layer, the photo-generated voltage at open-circuit state should be compensated by an applied voltage on both ends of the device to prevent charge combination. Applying voltage on spin photovoltaic devices generates an obvious current change from parallel magnetization to anti-parallel magnetization. Moreover, increasing the light irradiation power will further enhance the output current of the spin photovoltaic device. Therefore, rational control of external spin-polarized injection (tuning on applied voltage) and photo-generated carrier (tuning on light irradiation power) can produce totally spin-polarized current in the spin photovoltaic device.[85]

Although in this study only the n-type small molecule was employed, considering that n-type conjugated polymers have been successfully used to replace C_{60} and its derivatives in OPVs, we believe that n-type conjugated polymers are highly possible to be used in spin photovoltaic devices.

To date, n-type conjugated polymers are still rarely explored in the spintronic devices, including spin transport studies, organic spin-valves, and organic spin photovoltaics. However, some n-type conjugated polymers have already exhibited excellent magnetoresistance effects when integrated with FM electrodes.[92] The solution processability, tunable LUMO level and long spin diffusion lifetime of n-type conjugated polymers render them promising for application in organic spintronics. Notice that, different from OTE and OECT applications, organic spintronic devices always employed vertically sandwiched structures with thin active layer thickness; therefore, highly uniform and pin-hole free polymer films are desired. This requirement may need additional considerations when designing n-type conjugated polymers since many n-type conjugated polymers used in OFETs have high crystallinity and relatively rough surfaces.

5. n-Type conjugated polymers for energy storage

Recently, π-conjugated polymers are widely employed as the polymeric electrode in many energy-related applications, including supercapacitors and rechargeable batteries, by virtue of their intrinsic advantages of designable redox site, excellent electrochemical reversibility, high doping availability and theoretical capacity, flexibility, and cost-efficiency.[95,96] Generally, p-type

conjugated polymers are used accept anions when oxidized, and n-type conjugated polymers are used accept cations when reduced.[97] This electrochemical process, also seen as the doping or dedoping process, could be depicted as follows:

$$(\mathrm{p-CP})_n + nx\cdot\mathrm{Cl}^- \rightarrow [(\mathrm{p-CP})^{x+}\cdot x\mathrm{Cl}^-]_n + nx\cdot\mathrm{e}^-$$

$$(\mathrm{n-CP})_n + nx\cdot\mathrm{Li}^+ + nx\cdot\mathrm{e}^- \rightarrow [x\mathrm{Li}^+\cdot(\mathrm{n-CP})^{x-}]_n$$

where CP represents the conjugated polymer on the electrode and x is the doping level of the conjugated polymer. As shown in Fig. 9, the n-type conjugated polymer can serve as the anode like the conventional inorganic lithium anode to accept Li^+ cations and electrons, generating the Li-containing organic complex by doping the n-type conjugated polymer to a certain degree. On the other hand, during the discharging process, the Li-containing complex releases Li^+, and electrons flow through the external circuit.

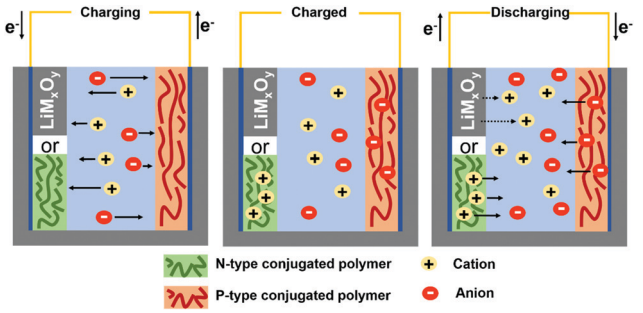

Fig. 9 Schematic illustration of the electron and ion migration process throughout a rechargeable electrochemical cell with polymeric electrodes, operating in three states: charging, charged and discharging.

Although polymeric electrodes applied in supercapacitors and rechargeable batteries have already shown excellent performance, there are still some bottlenecks restricting the further development in energy correlated applications. The first issue should be the possible destruction of the polymer chain upon a high level of doping.[98] Charging this conjugated polymer-based electrode with applied voltage over a certain limit will destroy the polymer structure, also called as overoxidation.[99,100] To overcome the unfavourable overoxidation process, the introduction of electron-withdrawing groups on the polymer backbone is proposed to enhance the stability upon reversible electrochemical charging and discharging.[103] The second issue is the limited amount of redox sites on typical p-type conjugated polymers. For example, polypyrrole could only accept 0.33 electron per repeat unit, and the maximum doping numbers for polythiophene, polyaniline, and PEDOT are all one electron, limiting their theoretical capacity ranging from 82 mA h g^{-1} to 295 mA h g^{-1}. Based on the above considerations, several n-type conjugated polymers were synthesized and employed as the polymeric anode to largely enhance the performance of rechargeable batteries and supercapacitors.[104–107]

Yao and Facchetti *et al.* used NDI based π-conjugated polymers for energy storage.[108] The alkyl side-chain grafted NDI acceptor unit was connected with the bithiophene donor to construct a D–A n-type conjugated polymer P(NDI2OD-T2), serving as the organic anode in rechargeable lithium batteries. As shown in Fig. 10b, two carbonyl groups of the NDI moiety are reduced with a high doping level of 2.0 through a two-step double lithium addition during electrochemical reduction. It is notable that this process is fully reversible and the electrons are delocalized across the polymer backbone by virtue of the π-conjugated system. However, overdoping on P(NDI2OD-T2) will induce irreversible structural deformation of the NDI moiety,

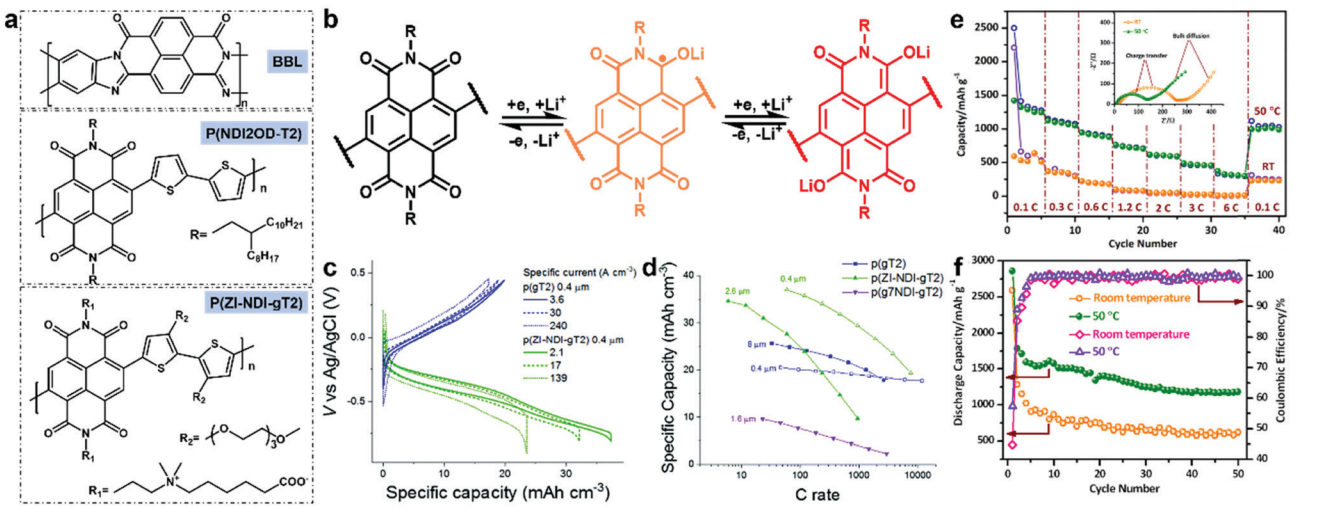

Fig. 10 (a) Chemical structures of several n-type conjugated polymers employed in rechargeable batteries and supercapacitors. (b) The two-step process of successive doping/lithiation of a NDI-based n-type conjugated polymer serving as the polymeric anode. (c) Galvanostatic charge–discharge curve of p-type polymer P(gT2) and n-type polymer P(ZI-NDI-gT2) upon different specific currents. (d) Rate performance of P(gT2), P(ZI-NDI-gT2) and P(g7NDI-gT2) with different film thickness during discharging.[101] Reprinted with permission from ref. 101, copyright 2018 The Royal Society of Chemistry. (e) Rate performance of the BBL-based anode at RT and 50 °C with the corresponding EIS diagrams (inset). (f) Cycling performance of the BBL-based anode on discharge capacity and coulombic efficiency.[102] Reprinted with permission from ref. 102, copyright 2018 Wiley-VCH.

impairing the battery performance. The specific capacity of P(NDI2OD-T2) reaches a value of 54.2 mA h g^{-1}, equalling the theoretical capacity of 2-electron reduction behavior. Fast charging–discharging measurements for the P(NDI2OD-T2) anode also show a high capacity retention of 99% at 10C and 79% at 500C, rendering the high potential of NDI-based n-type conjugated polymers in energy-related applications.

Recently, a new strategy was presented by Nelson *et al.* to develop a novel n-type conjugated polymer electrode for energy storage.[101] Specifically, the NDI unit was modified with a polar, zwitterionic side-chain to facilitate the ionic transport at the electrolyte–polymer interface during the charging and discharging process. The as-prepared n-type conjugated polymer P(ZI-NDI-gT2) electrode with large film thickness showed faster and more stable charging performance than the glycol side-chain modified polymer of P(g7NDI-gT2), as shown in Fig. 10c and d. The polymer with the glycol side-chain has stronger interactions with cations, whereas the zwitterionic side-chain has less, facilitating the ions to enter or escape from the polymer electrode. And thus the P(ZI-NDI-gT2) anode possesses better electrochemical behaviours during charging and discharging than the P(g7NDI-gT2) anode. Moreover, P(ZI-NDI-gT2) also exhibits two electron accepting capacity per unit during the charging process, and the NDI unit forms a bipolaron at −0.85 V *vs.* Ag/AgCl reference, which is consistent with the results reported by Yao and Facchetti *et al.*

BBL as a typical n-type conjugated polymer was also explored as the anode material in rechargeable Li batteries.[102] Zhang *et al.* synthesized two n-type ladder polymers, including BBL and its derivative SBBL. Both ladder-type polymers were dissolved in the strong protonic acid of methanesulfonic acid for processing. The BBL nanoparticle-based anode fabricated through the reprecipitation method exhibits strong Li-accepting capacity with about 44.7 Li ions per BBL unit. This result is consistent with the Li insertion model proposed by Sun *et al.*, who demonstrated that in fused aromatics, each C_6 ring can store up to six Li ions to form a 1 : 1 Li/C complex.[109] Therefore, the theoretical capacity of BBL could reach as high as 1926 mA h g^{-1}, equivalent to the maximum Li accepting number per BBL unit of 48. High-temperature operation (50 °C) of the BBL based battery contributes to overcoming the lithium insertion barrier to reach a higher discharge capacity and more excellent C-rate performance, as shown in Fig. 10e and f. The high specific capacity and thermal stability of the BBL anode remarkably promote the rapid development of n-type conjugated polymers applied in rechargeable Li batteries. Other n-type conjugated polymers, including poly(1,6-dihydropyrazino[2,3*g*]quinoxaline-2,3,8-triyl-7-(2*H*)-ylidene-7,8-dimethylidene) (PQL), polydopamine (PDA) and poly(1,4-dihydro-11*H*-pyrazino[2′,3′:3,4]cyclopenta [1,2-*b*]quinoxalin-11-one) (PPCQ), were also successfully employed as polymeric anodes in rechargeable batteries and supercapacitors with specific properties and high capacity performance, opening a new avenue for high-performance all-polymer energy storage and conversion systems.[104,105,110]

To gain a higher specific capacity, n-type conjugated polymers need (1) to possess more redox sites on the polymer backbone, (2) to be modified with electron-withdrawing groups to stabilize more electrons and Li cations in the polymer matrix, (3) to be grafted with hydrophilic side-chains to facilitate the water/ion uptake capacity for electrochemical energy storage, and (4) to be processed as nanostructured anode materials for capturing more ions in the electrolyte. Based on these requirements, traditional n-type conjugated polymer design strategies might not be suitable for the electrochemical energy storage applications; therefore, more efforts are needed to design novel polymer backbones and explore the electrochemical properties of n-type conjugated polymers.

6. Conclusion and outlook

During the past few years, n-type conjugated polymers have cut a brilliant figure in several emerging directions, such as OTEs, OECTs, organic spintronics, and organic energy storage systems. However the study of n-type conjugated polymers is still in a preliminary stage in many of these fields. We have noticed that each new research direction requires different molecular design considerations on n-type conjugated polymers. For instance, in OTEs, n-type conjugated polymers with lower LUMO level, higher electron mobility, and better mixing with dopant are favoured; the requirements of OECTs are similar in many aspects, but hydrophilicity and ion diffusion/penetration are more important factors. Both OECTs and organic rechargeable batteries need conjugated polymers to directly contact an electrolyte, where ion and electron transport are critical in both devices. To a certain content, the molecular design and device optimization in OECTs and rechargeable batteries might have some similarities. However, in OECTs, charge transport is more important, whereas in electrochemical systems, charge storage capacity is the first priority. For spintronics, modulating the LUMO level to match the Fermi level of FM electrodes and obtaining higher electron mobility are critical factors, but spintronics seems to require better film quality before the device can be successfully fabricated.

Owing to the rapid development of n-type conjugated polymers in the past few years, many new building blocks and design strategies have been proposed to meet the various requirements in these emerging directions. The stability issue of n-type conjugated polymers is also progressively being solved. Since many of these emerging research directions share many similarities in both molecular structures and working mechanisms, we believe that if the fruitful achievements from conventional n-type conjugated polymer studies can be translated into these directions, more significant advances will be made in these new research directions.

Conflicts of interest

There are no conflicts to declare.

Acknowledgements

This work is supported by the Beijing Natural Science Foundation (2192020), in part by the Guangdong Science and Technology Project (2019B010934001).

References

1 J. Yang, Z. Y. Zhao, S. Wang, Y. L. Guo and Y. Q. Liu, *Chem*, 2018, **4**, 2748.
2 X. Zhao and X. Zhan, *Chem. Soc. Rev.*, 2011, **40**, 3728.
3 G. Zhang, J. Zhao, P. C. Y. Chow, K. Jiang, J. Zhang, Z. Zhu, J. Zhang, F. Huang and H. Yan, *Chem. Rev.*, 2018, **118**, 3447.
4 M. Kaltenbrunner, M. S. White, E. D. Glowacki, T. Sekitani, T. Someya, N. S. Sariciftci and S. Bauer, *Nat. Commun.*, 2012, **3**, 770.
5 Y. Zhao, Y. Guo and Y. Liu, *Adv. Mater.*, 2013, **25**, 5372.
6 S. Holliday, J. E. Donaghey and I. McCulloch, *Chem. Mater.*, 2013, **26**, 647.
7 H. Klauk, *Chem. Soc. Rev.*, 2010, **39**, 2643.
8 A. Pron, P. Gawrys, M. Zagorska, D. Djurado and R. Demadrille, *Chem. Soc. Rev.*, 2010, **39**, 2577.
9 J. S. Wu, S. W. Cheng, Y. J. Cheng and C. S. Hsu, *Chem. Soc. Rev.*, 2015, **44**, 1113.
10 H. Benten, D. Mori, H. Ohkita and S. Ito, *J. Mater. Chem. A*, 2016, **4**, 5340.
11 R. S. Gurney, D. G. Lidzey and T. Wang, *Rep. Prog. Phys.*, 2019, **82**, 036601.
12 A. Tsumura, H. Koezuka and T. Ando, *Appl. Phys. Lett.*, 1986, **49**, 1210.
13 G. Yu, J. Gao, J. C. Hummelen, F. Wudl and A. J. Heeger, *Science*, 1995, **270**, 1789.
14 I. Osaka, K. Takimiya and R. D. McCullough, *Adv. Mater.*, 2010, **22**, 4993.
15 T. Lei, Y. Cao, Y. Fan, C. J. Liu, S. C. Yuan and J. Pei, *J. Am. Chem. Soc.*, 2011, **133**, 6099.
16 I. Kang, H. J. Yun, D. S. Chung, S. K. Kwon and Y. H. Kim, *J. Am. Chem. Soc.*, 2013, **135**, 14896.
17 G. Kim, S. J. Kang, G. K. Dutta, Y. K. Han, T. J. Shin, Y. Y. Noh and C. Yang, *J. Am. Chem. Soc.*, 2014, **136**, 9477.
18 C. Luo, A. K. Kyaw, L. A. Perez, S. Patel, M. Wang, B. Grimm, G. C. Bazan, E. J. Kramer and A. J. Heeger, *Nano Lett.*, 2014, **14**, 2764.
19 J. Li, Y. Zhao, H. S. Tan, Y. Guo, C. A. Di, G. Yu, Y. Liu, M. Lin, S. H. Lim, Y. Zhou, H. Su and B. S. Ong, *Sci. Rep.*, 2012, **2**, 754.
20 X. Z. Che, Y. X. Li, Y. Qu and S. R. Forrest, *Nat. Energy*, 2018, **3**, 422.
21 Y. Cui, H. Yao, J. Zhang, T. Zhang, Y. Wang, L. Hong, K. Xian, B. Xu, S. Zhang, J. Peng, Z. Wei, F. Gao and J. Hou, *Nat. Commun.*, 2019, **10**, 2515.
22 J. Yuan, Y. Zhang, L. Zhou, G. Zhang, H.-L. Yip, T.-K. Lau, X. Lu, C. Zhu, H. Peng, P. A. Johnson, M. Leclerc, Y. Cao, J. Ulanski, Y. Li and Y. Zou, *Joule*, 2019, **3**, 1140.
23 H. Usta, A. Facchetti and T. J. Marks, *Acc. Chem. Res.*, 2011, **44**, 501.
24 Z. T. Liu, D. Zeng, X. Gao, P. C. Li, Q. Zhang and X. Peng, *Sol. Energy Mater. Sol. Cells*, 2019, **189**, 103.
25 Y. Guo, Y. Li, O. Awartani, H. Han, J. Zhao, H. Ade, H. Yan and D. Zhao, *Adv. Mater.*, 2017, **29**, 1700309.
26 R. Di Pietro, D. Fazzi, T. B. Kehoe and H. Sirringhaus, *J. Am. Chem. Soc.*, 2012, **134**, 14877.
27 H. Usta, C. Risko, Z. Wang, H. Huang, M. K. Deliomeroglu, A. Zhukhovitskiy, A. Facchetti and T. J. Marks, *J. Am. Chem. Soc.*, 2009, **131**, 5586.
28 G. Zuo, M. Linares, T. Upreti and M. Kemerink, *Nat. Mater.*, 2019, **18**, 588.
29 Y. Q. Zheng, T. Lei, J. H. Dou, X. Xia, J. Y. Wang, C. J. Liu and J. Pei, *Adv. Mater.*, 2016, **28**, 7213.
30 Z. Zhao, Z. Yin, H. Chen, L. Zheng, C. Zhu, L. Zhang, S. Tan, H. Wang, Y. Guo, Q. Tang and Y. Liu, *Adv. Mater.*, 2017, **29**, 1602410.
31 C. J. Mueller, C. R. Singh, M. Fried, S. Huettner and M. Thelakkat, *Adv. Funct. Mater.*, 2015, **25**, 2725.
32 T. Lei, X. Xia, J. Y. Wang, C. J. Liu and J. Pei, *J. Am. Chem. Soc.*, 2014, **136**, 2135.
33 T. Lei, J. H. Dou, Z. J. Ma, C. H. Yao, C. J. Liu, J. Y. Wang and J. Pei, *J. Am. Chem. Soc.*, 2012, **134**, 20025.
34 S. Lan, Y. Yan, H. Yang, G. Zhang, Y. Ye, F. Li, H. Chen and T. Guo, *J. Mater. Chem. C*, 2019, **7**, 4543.
35 J. Liu, Z. Qin, H. Gao, H. Dong, J. Zhu and W. Hu, *Adv. Funct. Mater.*, 2019, **29**, 1808453.
36 A. J. Ben-Sasson, D. Azulai, H. Gilon, A. Facchetti, G. Markovich and N. Tessler, *ACS Appl. Mater. Interfaces*, 2015, **7**, 2149.
37 B. Sun, W. Hong, Z. Yan, H. Aziz and Y. Li, *Adv. Mater.*, 2014, **26**, 2636.
38 K. Guo, J. H. Bai, Y. Jiang, Z. L. Wang, Y. Sui, Y. F. Deng, Y. Han, H. K. Tian and Y. H. Geng, *Adv. Funct. Mater.*, 2018, **28**, 1801097.
39 C. Zhu, Z. Zhao, H. Chen, L. Zheng, X. Li, J. Chen, Y. Sun, F. Liu, Y. Guo and Y. Liu, *J. Am. Chem. Soc.*, 2017, **139**, 17735.
40 B. Fan, L. Ying, P. Zhu, F. Pan, F. Liu, J. Chen, F. Huang and Y. Cao, *Adv. Mater.*, 2017, **29**, 1703906.
41 J. T. E. Quinn, J. X. Zhu, X. Li, J. L. Wang and Y. N. Li, *J. Mater. Chem. C*, 2017, **5**, 8654.
42 Y. Wang and T. Michinobu, *J. Mater. Chem. C*, 2018, **6**, 10390.
43 B. Russ, A. Glaudell, J. J. Urban, M. L. Chabinyc and R. A. Segalman, *Nat. Rev. Mater.*, 2016, **1**, 16050.
44 O. Bubnova and X. Crispin, *Energy Environ. Sci.*, 2012, **5**, 9345.
45 M. Bharti, A. Singh, S. Samanta and D. K. Aswal, *Prog. Mater. Sci.*, 2018, **93**, 270.
46 C. Y. Yang, W. L. Jin, J. Wang, Y. F. Ding, S. Nong, K. Shi, Y. Lu, Y. Z. Dai, F. D. Zhuang, T. Lei, C. A. Di, D. Zhu, J. Y. Wang and J. Pei, *Adv. Mater.*, 2018, **30**, e1802850.
47 H. Yao, Z. Fan, H. Cheng, X. Guan, C. Wang, K. Sun and J. Ouyang, *Macromol. Rapid Commun.*, 2018, **39**, e1700727.
48 T. Park, C. Park, B. Kim, H. Shin and E. Kim, *Energy Environ. Sci.*, 2013, **6**, 788.
49 O. Bubnova, Z. U. Khan, H. Wang, S. Braun, D. R. Evans, M. Fabretto, P. Hojati-Talemi, D. Dagnelund, J. B. Arlin, Y. H. Geerts, S. Desbief, D. W. Breiby, J. W. Andreasen, R. Lazzaroni, W. M. Chen, I. Zozoulenko, M. Fahlman, P. J. Murphy, M. Berggren and X. Crispin, *Nat. Mater.*, 2014, **13**, 190.

50 O. Bubnova, Z. U. Khan, A. Malti, S. Braun, M. Fahlman, M. Berggren and X. Crispin, *Nat. Mater.*, 2011, **10**, 429.
51 G. H. Kim, L. Shao, K. Zhang and K. P. Pipe, *Nat. Mater.*, 2013, **12**, 719.
52 L. E. Bell, *Science*, 2008, **321**, 1457.
53 Y. Sun, P. Sheng, C. Di, F. Jiao, W. Xu, D. Qiu and D. Zhu, *Adv. Mater.*, 2012, **24**, 932.
54 R. A. Schlitz, F. G. Brunetti, A. M. Glaudell, P. L. Miller, M. A. Brady, C. J. Takacs, C. J. Hawker and M. L. Chabinyc, *Adv. Mater.*, 2014, **26**, 2825.
55 S. Wang, H. Sun, U. Ail, M. Vagin, P. O. Persson, J. W. Andreasen, W. Thiel, M. Berggren, X. Crispin, D. Fazzi and S. Fabiano, *Adv. Mater.*, 2016, **28**, 10764.
56 K. Shi, F. Zhang, C. A. Di, T. W. Yan, Y. Zou, X. Zhou, D. Zhu, J. Y. Wang and J. Pei, *J. Am. Chem. Soc.*, 2015, **137**, 6979.
57 X. Zhao, D. Madan, Y. Cheng, J. Zhou, H. Li, S. M. Thon, A. E. Bragg, M. E. DeCoster, P. E. Hopkins and H. E. Katz, *Adv. Mater.*, 2017, **29**, 1606928.
58 J. Liu, L. Qiu, R. Alessandri, X. Qiu, G. Portale, J. Dong, W. Talsma, G. Ye, A. A. Sengrian, P. C. T. Souza, M. A. Loi, R. C. Chiechi, S. J. Marrink, J. C. Hummelen and L. J. A. Koster, *Adv. Mater.*, 2018, **30**, 1704630.
59 S. Wang, H. Sun, T. Erdmann, G. Wang, D. Fazzi, U. Lappan, Y. Puttisong, Z. Chen, M. Berggren, X. Crispin, A. Kiriy, B. Voit, T. J. Marks, S. Fabiano and A. Facchetti, *Adv. Mater.*, 2018, **30**, e1801898.
60 D. Nava, Y. Shin, M. Massetti, X. Jiao, T. Biskup, M. S. Jagadeesh, A. Calloni, L. Duo, G. Lanzani, C. R. McNeill, M. Sommer and M. Caironi, *ACS Appl. Energy Mater.*, 2018, **1**, 4626.
61 S. Inal, J. Rivnay, A. O. Suiu, G. G. Malliaras and I. McCulloch, *Acc. Chem. Res.*, 2018, **51**, 1368.
62 H. Sun, M. Vagin, S. Wang, X. Crispin, R. Forchheimer, M. Berggren and S. Fabiano, *Adv. Mater.*, 2018, **30**, 1704916.
63 Y. van de Burgt, E. Lubberman, E. J. Fuller, S. T. Keene, G. C. Faria, S. Agarwal, M. J. Marinella, A. Alec Talin and A. Salleo, *Nat. Mater.*, 2017, **16**, 414.
64 J. Rivnay, S. Inal, A. Salleo, R. M. Owens, M. Berggren and G. G. Malliaras, *Nat. Rev. Mater.*, 2018, **3**, 17086.
65 O. Parlak, S. T. Keene, A. Marais, V. F. Curto and A. Salleo, *Sci. Adv.*, 2018, **4**, eaar2904.
66 W. Xu, S. Y. Min, H. Hwang and T. W. Lee, *Sci. Adv.*, 2016, **2**, e1501326.
67 E. Zeglio and O. Inganas, *Adv. Mater.*, 2018, **30**, e1800941.
68 R. Giridharagopal, L. Q. Flagg, J. S. Harrison, M. E. Ziffer, J. Onorato, C. K. Luscombe and D. S. Ginger, *Nat. Mater.*, 2017, **16**, 737.
69 A. Laiho, L. Herlogsson, R. Forchheimer, X. Crispin and M. Berggren, *Proc. Natl. Acad. Sci. U. S. A.*, 2011, **108**, 15069.
70 M. Moser, J. F. Ponder, A. Wadsworth, A. Giovannitti and I. McCulloch, *Adv. Funct. Mater.*, 2018, **29**, 1807033.
71 D. A. Bernards and G. G. Malliaras, *Adv. Funct. Mater.*, 2007, **17**, 3538.
72 S. M. Kim, C. H. Kim, Y. Kim, N. Kim, W. J. Lee, E. H. Lee, D. Kim, S. Park, K. Lee, J. Rivnay and M. H. Yoon, *Nat. Commun.*, 2018, **9**, 3858.
73 L. Q. Flagg, C. G. Bischak, J. W. Onorato, R. B. Rashid, C. K. Luscombe and D. S. Ginger, *J. Am. Chem. Soc.*, 2019, **141**, 4345.
74 A. Giovannitti, D. T. Sbircea, S. Inal, C. B. Nielsen, E. Bandiello, D. A. Hanifi, M. Sessolo, G. G. Malliaras, I. McCulloch and J. Rivnay, *Proc. Natl. Acad. Sci. U. S. A.*, 2016, **113**, 12017.
75 L. R. Savagian, A. M. Osterholm, J. F. Ponder, Jr., K. J. Barth, J. Rivnay and J. R. Reynolds, *Adv. Mater.*, 2018, **30**, e1804647.
76 A. Giovannitti, K. J. Thorley, C. B. Nielsen, J. Li, M. J. Donahue, G. G. Malliaras, J. Rivnay and I. McCulloch, *Adv. Funct. Mater.*, 2018, **28**, 1706325.
77 C. B. Nielsen, A. Giovannitti, D. T. Sbircea, E. Bandiello, M. R. Niazi, D. A. Hanifi, M. Sessolo, A. Amassian, G. G. Malliaras, J. Rivnay and I. McCulloch, *J. Am. Chem. Soc.*, 2016, **138**, 10252.
78 H. D. Sun, J. Gerasimov, M. Berggren and S. Fabiano, *J. Mater. Chem. C*, 2018, **6**, 11778.
79 A. Giovannitti, C. B. Nielsen, D. T. Sbircea, S. Inal, M. Donahue, M. R. Niazi, D. A. Hanifi, A. Amassian, G. G. Malliaras, J. Rivnay and I. McCulloch, *Nat. Commun.*, 2016, **7**, 13066.
80 A. Giovannitti, I. P. Maria, D. Hanifi, M. J. Donahue, D. Bryant, K. J. Barth, B. E. Makdah, A. Savva, D. Moia, M. Zetek, P. R. F. Barnes, O. G. Reid, S. Inal, G. Rumbles, G. G. Malliaras, J. Nelson, J. Rivnay and I. McCulloch, *Chem. Mater.*, 2018, **30**, 2945.
81 A. M. Pappa, D. Ohayon, A. Giovannitti, I. P. Maria, A. Savva, I. Uguz, J. Rivnay, I. McCulloch, R. M. Owens and S. Inal, *Sci. Adv.*, 2018, **4**, eaat0911.
82 M. J. Donahue, A. Williamson, X. Strakosas, J. T. Friedlein, R. R. McLeod, H. Gleskova and G. G. Malliaras, *Adv. Mater.*, 2018, **30**, 1705031.
83 J. P. Prieto-Ruiz, S. G. Miralles, H. Prima-Garcia, A. Lopez-Munoz, A. Riminucci, P. Graziosi, M. Aeschlimann, M. Cinchetti, V. A. Dediu and E. Coronado, *Adv. Mater.*, 2019, **31**, e1806817.
84 J. Y. Hong, K. H. O. Yang, B. Y. Wang, K. S. Li, H. W. Shiu, C. H. Chen, Y. L. Chan, D. H. Wei, F. H. Chang, H. J. Lin, W. C. Chiang and M. T. Lin, *Appl. Phys. Lett.*, 2014, **104**, 083301.
85 X. Sun, S. Velez, A. Atxabal, A. Bedoya-Pinto, S. Parui, X. Zhu, R. Llopis, F. Casanova and L. E. Hueso, *Science*, 2017, **357**, 677.
86 V. Dediu, M. Murgia, F. C. Matacotta, C. Taliani and S. Barbanera, *Solid State Commun.*, 2002, **122**, 181.
87 R. Kienberger, E. Goulielmakis, M. Uiberacker, A. Baltuska, V. Yakovlev, F. Bammer, A. Scrinzi, T. Westerwalbesloh, U. Kleineberg, U. Heinzmann, M. Drescher and F. Krausz, *Nature*, 2004, **427**, 817.
88 J. Devkota, R. G. Geng, R. C. Subedi and T. D. Nguyen, *Adv. Funct. Mater.*, 2016, **26**, 3881.
89 F. Li, T. Li, F. Chen and F. Zhang, *Sci. Rep.*, 2015, **5**, 9355.
90 D. Sun, K. J. van Schooten, M. Kavand, H. Malissa, C. Zhang, M. Groesbeck, C. Boehme and Z. Valy Vardeny, *Nat. Mater.*, 2016, **15**, 863.

91 S. J. Wang, D. Venkateshvaran, M. R. Mahani, U. Chopra, E. R. McNellis, R. Di Pietro, S. Schott, A. Wittmann, G. Schweicher, M. Cubukcu, K. Kang, R. Carey, T. J. Wagner, J. N. M. Siebrecht, D. P. G. H. Wong, I. E. Jacobs, R. O. Aboljadayel, A. Ionescus, S. A. Egorov, S. Mueller, O. Zadvorna, P. Skalski, C. Jellett, M. Little, A. Marks, I. McCulloch, J. Wunderlich, J. Sinova and H. Sirringhaus, *Nat. Electron.*, 2019, **2**, 98.
92 G. Q. Zhou, G. Q. Tang, T. Li, G. X. Pan, Z. H. Deng and F. P. Zhang, *J. Phys. D: Appl. Phys.*, 2017, **50**, 095001.
93 Y. H. Liu, T. Lee, H. E. Katz and D. H. Reich, *J. Appl. Phys.*, 2009, **105**, 07c708.
94 S. Watanabe, K. Ando, K. Kang, S. Mooser, Y. Vaynzof, H. Kurebayashi, E. Saitoh and H. Sirringhaus, *Nat. Phys.*, 2014, **10**, 308.
95 S. Muench, A. Wild, C. Friebe, B. Haupler, T. Janoschka and U. S. Schubert, *Chem. Rev.*, 2016, **116**, 9438.
96 Z. P. Song and H. S. Zhou, *Energy Environ. Sci.*, 2013, **6**, 2280.
97 M. Berggren and G. G. Malliaras, *Science*, 2019, **364**, 233.
98 Q. Zhao, Z. Zhu and J. Chen, *Adv. Mater.*, 2017, **29**, 1607007.
99 S. Ghosh, G. A. Bowmaker, R. P. Cooney and J. M. Seakins, *Synth. Met.*, 1998, **95**, 63.
100 A. Zykwinska, W. Domagala, B. Pilawa and M. Lapkowski, *Electrochim. Acta*, 2005, **50**, 1625.
101 D. Moia, A. Giovannitti, A. A. Szumska, I. P. Maria, E. Rezasoltani, M. Sachs, M. Schnurr, P. R. F. Barnes, I. McCulloch and J. Nelson, *Energy Environ. Sci.*, 2019, **12**, 1349.
102 J. S. Wu, X. H. Rui, C. Y. Wang, W. B. Pei, R. Lau, Q. Y. Yan and Q. C. Zhang, *Adv. Energy Mater.*, 2015, **5**, 1402189.
103 J. Xie, P. Y. Gu and Q. C. Zhang, *ACS Energy Lett.*, 2017, **2**, 1985.
104 T. Sun, Z. J. Li, H. G. Wang, D. Bao, F. L. Meng and X. B. Zhang, *Angew. Chem., Int. Ed.*, 2016, **55**, 10662.
105 J. Wu, X. Rui, G. Long, W. Chen, Q. Yan and Q. Zhang, *Angew. Chem., Int. Ed.*, 2015, **54**, 7354.
106 S. Sharma, R. Soni, S. Kurungot and S. K. Asha, *J. Phys. Chem. C*, 2019, **123**, 2084.
107 B. T. McAllister, T. B. Schon, P. M. DiCarmine and D. S. Seferos, *Polym. Chem.*, 2017, **8**, 5194.
108 Y. Liang, Z. Chen, Y. Jing, Y. Rong, A. Facchetti and Y. Yao, *J. Am. Chem. Soc.*, 2015, **137**, 4956.
109 X. Han, G. Qing, J. Sun and T. Sun, *Angew. Chem., Int. Ed.*, 2012, **51**, 5147.
110 J. Xie, X. Rui, P. Gu, J. Wu, Z. J. Xu, Q. Yan and Q. Zhang, *ACS Appl. Mater. Interfaces*, 2016, **8**, 16932.